Fabrication and Thermoelectric Properties of Freestanding $Ba_{1/3}CoO_2$ Single Crystalline Films

Kungwan Kang[1], Fumiaki Kato[2], Akitoshi Nakano[2], Ichiro Terasaki[2,*], Takashi Endo[3], Yasutaka Matsuo[3], Hyoungjeen Jeen[4,*], and Hiromichi Ohta[3,*]

[1] *Graduate School of Information Science and Technology, Hokkaido University, N14W9, Kita, Sapporo 060-0814, Japan*

[2] *Department of Physics, Nagoya University, Furo, Chikusa, Nagoya 464-8602, Japan*

[3] *Research Institute for Electronic Science, Hokkaido University, N20W10, Kita, Sapporo 001-0020, Japan*

[4] *Department of Physics, Pusan National University, Geumjeong-gu, Busan 46241, Korea*

*Emails: terra@nagoya-u.jp, hjeen@pusan.ac.kr, hiromichi.ohta@es.hokudai.ac.jp

KEYWORDS: thermoelectric properties, $Ba_{1/3}CoO_2$, single crystalline, freestanding film, peeled off

ABSTRACT: Thermoelectric energy conversion has attracted attention as an energy-harvesting technology for converting waste heat into electricity via the Seebeck effect. Conducting oxide-based thermoelectric materials that exhibit a high figure of merit are promising because of their good chemical and thermal stability, as well as their harmless nature compared to chalcogenide-based state-of-the-art thermoelectric materials. Among

many conducting oxides, $Ba_{1/3}CoO_2$ epitaxial films exhibit the highest figures of merit. For the practical use of $Ba_{1/3}CoO_2$, bulk ceramics or single-crystalline $Ba_{1/3}CoO_2$ are necessary. Here, we show that freestanding $Ba_{1/3}CoO_2$ single-crystalline films can be fabricated by peeling $Ba_{1/3}CoO_2$ epitaxial films from the substrate. We fabricated $Ba_{1/3}CoO_2$ epitaxial films and immersed them in 40 °C hot water for several tens of minutes. Subsequently, the $Ba_{1/3}CoO_2$ epitaxial film spontaneously peeled off and floated on the surface of the water like seaweed. We measured and analyzed the crystal structure, chemical composition, and thermoelectric properties before and after peeling and realized that there was no significant difference. The present results would provide a useful method for fabricating freestanding single-crystalline oxide films for thermoelectrics.

INTRODUCTION

Thermoelectric devices convert a temperature difference into an electric current and vice versa based on the Seebeck effect/Peltier effect.[1, 2] They have potential as environmentally friendly energy harvesting technologies because they convert waste heat into useful electricity. Their performance is expressed by the dimensionless figure of merit (*ZT*), which is given as $S^2 \cdot \sigma \cdot T \cdot \kappa^{-1}$, where S is the thermopower, σ is the electrical conductivity, T is the absolute temperature, and κ is the thermal conductivity.[1, 3] Although several metal chalcogenides including Bi_2Te_3,[4-6] PbTe,[7, 8] and SnSe[9-11] exhibit rather high *ZT* (>2), they are not environmentally benign because of their chemical and thermal instabilities. In this regard, several conducting metal oxides[12-16] have attracted significant attention as potential thermoelectric materials.

Among the many conducting metal oxides, we focus on $Ba_{1/3}CoO_2$[17, 18]. $Ba_{1/3}CoO_2$ is a layered material composed of alternating CoO_2 and Ba layers stacked along the *c*-axis. $Ba_{1/3}CoO_2$ exhibited metallic p-type conductivity up to 600 °C in air. Recently, we found that $Ba_{1/3}CoO_2$ epitaxial films exhibit a large *ZT* of 0.11 at room temperature[19] and 0.55 at 600 °C.[20] These values are the highest among reliable oxide thermoelectric materials and are comparable to those of commercially available p-type PbTe and SiGe.[1] However, $Ba_{1/3}CoO_2$ epitaxial films possess a serious drawback, i.e., because the substrate (α-Al_2O_3 or YSZ) is an electrical insulator, the overall *ZT* including the substrate is extremely low. Thus, the

fabrication of bulk ceramics and single-crystalline $Ba_{1/3}CoO_2$ is crucial. Liu *et al*. fabricated $Ba_{1/3}CoO_2$ ceramics and measured their *ZT* at several temperatures.[17, 18] However, the *ZT* of the ceramics was only 0.005 at room temperature, which is more than one order of magnitude lower than that of epitaxial films, probably because of the suppression of electron transport at the grain boundaries (grain boundary scattering).

Recently, peeling off of the epitaxial films of perovskite oxides has been studied intensively.[21-23] As the sacrificial layer, water-soluble $Sr_3Al_2O_6$ films are epitaxially grown on the substrate before the perovskite oxide film growth; then, the perovskite oxide film is peeled off by dissolving the sacrificial layers in water.[21] Ohta *et al*. reported that $Na_{3/4}CoO_2$ epitaxial film grown on (0001) α-Al_2O_3 peels off when immersed in water because a water-soluble amorphous Na-Al-O layer spontaneously forms at the interface between $Na_{3/4}CoO_2$ epitaxial film and α-Al_2O_3 substrate.[24] Thus, the amorphous Na-Al-O layer acts as the sacrificial layer. In the case of $Ba_{1/3}CoO_2$ epitaxial films, an amorphous Ba-Al-O layer is spontaneously formed at the interface between $Ba_{1/3}CoO_2$ epitaxial film and α-Al_2O_3 substrate.[19] Therefore, we expect that the amorphous Ba-Al-O layer acts as the sacrificial layer and freestanding $Ba_{1/3}CoO_2$ epitaxial film would be obtained.

Here, we show that freestanding $Ba_{1/3}CoO_2$ single-crystalline films can be fabricated by peeling $Ba_{1/3}CoO_2$ epitaxial films from the substrate. We fabricated $Ba_{1/3}CoO_2$ epitaxial films and immersed them in 40 °C hot water for several tens of minutes. Subsequently, the $Ba_{1/3}CoO_2$ epitaxial film spontaneously peeled off and floated on the surface of the water like seaweed. We measured and analyzed the crystal structure, chemical composition, and thermoelectric properties before and after peeling and realized that there was no significant difference. The results of this study provide a useful method for fabricating freestanding single-crystalline oxide films for thermoelectrics.

RESULTS AND DISCUSSION

First, $Ba_{1/3}CoO_2$ epitaxial films (~600 nm) were fabricated on (0001) α-Al_2O_3 substrates by the reactive solid-phase epitaxy (R-SPE) method[25] and a subsequent ion exchange treatment.

The fabrication procedure of $Ba_{1/3}CoO_2$ epitaxial films has been reported elsewhere.[19, 20] During the R-SPE and the ion exchange treatment, a ~10-nm-thick amorphous Ba-Al-O layer formed spontaneously at the interface between the $Ba_{1/3}CoO_2$ film and the α-Al_2O_3 substrate.[18] We confirmed that the crystallographic feature and the thermoelectric properties are consistent with previous reports.[19, 20]

The $Ba_{1/3}CoO_2$ epitaxial film was then peeled from the α-Al_2O_3 substrate, as shown schematically in **Fig. 1a**. First, we immersed the $Ba_{1/3}CoO_2$ epitaxial film in hot water (40 °C). Before immersion in water, it was difficult for the $Ba_{1/3}CoO_2$ epitaxial film to attach to the substrate (**Fig. 1b**). Several tens of minutes later, the amorphous Ba-Al-O layer dissolved and the $Ba_{1/3}CoO_2$ epitaxial film peeled off. Subsequently, the peeled-off $Ba_{1/3}CoO_2$ epitaxial film floated on the surface of the water (**Fig. 1c**), similar to seaweed. To measure the properties of the peeled $Ba_{1/3}CoO_2$ epitaxial film, we pasted it onto a glass substrate and air-dried it at room temperature (**Fig. 1d**). The film was flexible when thin plastic substrates were used instead of glass substrates (data not shown).

High-resolution X-ray diffraction measurements of the peeled-off $Ba_{1/3}CoO_2$ epitaxial film were performed. **Figure 2** shows the out-of-plane XRD patterns of the as-grown and peeled-off $Ba_{1/3}CoO_2$ epitaxial films. The peeled-off $Ba_{1/3}CoO_2$ epitaxial film exhibited only intense Bragg diffraction peaks for 000*l* $Ba_{1/3}CoO_2$ (**Fig. 2c**). The position and intensity of the Bragg diffraction peaks did not change compared to those of the as-grown $Ba_{1/3}CoO_2$ epitaxial film (**Fig. 2a**), except that the substrate peak disappeared. *c*-axis lattice parameter of the peeled $Ba_{1/3}CoO_2$ epitaxial film was 1.221 nm. The full width at half maximum (FWHM) of the out-of-plane X-ray rocking curve (OXRC) of 0002 $Ba_{1/3}CoO_2$ was ~2.0° (**Fig. 2d**), which is slightly wider than that of the as-grown film (~1.7°). Compared with a previous report[19], the FHWM of the OXRC was significantly wider (this work: ~2.0°, previous report: ~0.8°), probably because the thickness is three times greater (this work:600 nm, previous report:200 nm). We further measured the chemical composition of the peeled-off $Ba_{1/3}CoO_2$ epitaxial film using inductively coupled plasma mass spectrometry (ICP-MS) and obtained a Ba/Co ratio of 0.323. These results reveal that the peel-off treatment does not affect the chemical composition or crystal structure of the $Ba_{1/3}CoO_2$ epitaxial films.

We then observed the microstructure of the peeled-off $Ba_{1/3}CoO_2$ epitaxial film using high-angle annular dark-field (HAADF) scanning transmission electron microscopy (STEM). **Figure 3a** shows a cross-sectional HAADF-STEM image of a peeled $Ba_{1/3}CoO_2$ epitaxial film. The overall thickness of the $Ba_{1/3}CoO_2$ film was approximately 600 nm, which is consistent with the designed thickness. **Figure 3b** shows a magnified HAADF-STEM image. The incident direction of the e-beam corresponded to the $[11\bar{2}0]$ of the peeled-off $Ba_{1/3}CoO_2$ epitaxial film. The crystal structure was composed of alternating CoO_2 (blue circles) and Ba (yellow circles) layers.

Next, we measured the thermoelectric properties of the freestanding $Ba_{1/3}CoO_2$ single-crystalline films in the in-plane direction. The room-temperature electrical conductivity (σ) of the as-grown $Ba_{1/3}CoO_2$ film was ~1100 S cm^{-1}, while that of freestanding $Ba_{1/3}CoO_2$ single crystalline film was ~1000 S cm^{-1}. Both films exhibited metallic conductivity, in which the σ increased as the temperature decreased (**Fig. 4a**). Note that σ of the freestanding $Ba_{1/3}CoO_2$ single crystalline film is significantly lower than that of the previous report (σ: 2300 S cm^{-1})[19]. This may be because the crystalline tilting of the freestanding $Ba_{1/3}CoO_2$ single-crystal film was larger than that in the previous report; therefore, grain boundary scattering contributes significantly[26]. The room-temperature S of the as-grown $Ba_{1/3}CoO_2$ film was +76 μV K^{-1}, while that of the freestanding $Ba_{1/3}CoO_2$ single crystalline film was +73 μV K^{-1}. The S values of both films gradually decreased as the temperature decreased (**Fig. 4b**), demonstrating that the peeling treatment did not affect the thermoelectric properties.

Finally, we measured the thermal conductivity (κ) of the freestanding $Ba_{1/3}CoO_2$ single crystalline films. κ is expressed by $\kappa = C_p \cdot \rho \cdot D$, where C_p is the specific heat capacity, ρ is the bulk density, and D is the thermal diffusivity. Because C_p (0.44 J g^{-1} K^{-1}) and ρ (5.36 g cm^{-3}) at room temperature are known, we measured D of the freestanding $Ba_{1/3}CoO_2$ single crystalline films at room temperature using the AC calorimetric method.[27, 28] First, we fixed the sample between a Peltier device and a Cu plate using Ag paste (**Fig. 5**). We then applied an AC heat flux to the sample using the Peltier device and measured the temperature at position x using an IR camera. **Supporting Information** provides details of our AC

calorimetric method.

The AC calorimetric measurements indicated that the freestanding $Ba_{1/3}CoO_2$ single-crystalline films had D of 1.45 mm^2/s at room temperature (**Fig. 6**). Consequently, the obtained κ for the freestanding $Ba_{1/3}CoO_2$ single crystalline films of ~3.4 W m^{-1} K^{-1} agreed well with that of the as-grown film (~3.2 W m^{-1} K^{-1})[19]. For comparison, we measured κ of a freestanding $Sr_{1/3}CoO_2$ single crystalline film, which was prepared in a similar manner as $Ba_{1/3}CoO_2$. Consistent with the as-grown film (~4.4 W m^{-1} K^{-1}),[19] the obtained κ was ~4.1 W m^{-1} K^{-1}.

Here, we summarize the thermoelectric properties of freestanding $Ba_{1/3}CoO_2$ single crystalline films (**Table 1**). From these results, we conclude that we successfully fabricated freestanding $Ba_{1/3}CoO_2$ single-crystalline films that exhibited a thermoelectric ZT of 0.047 at room temperature. Compared to a previous report ($Ba_{1/3}CoO_2$ single crystalline films on (0001) α-Al_2O_3 substrate),[19] ZT of the present freestanding $Ba_{1/3}CoO_2$ single crystalline films is significantly lower due to a lower σ. Except for σ, the thermoelectric properties of the freestanding $Ba_{1/3}CoO_2$ single crystalline films are similar to that in the previous report.[19] Because grain boundary scattering dominantly occurs at lower temperatures[26], the larger grain boundary angle of the freestanding $Ba_{1/3}CoO_2$ single crystalline film suppresses σ. Owing to the similar origin, σ of the $Ba_{1/3}CoO_2$ films grown on YSZ substrates showed a lower σ (1100 S cm^{-1} [20]) than that of $Ba_{1/3}CoO_2$ films on (0001) α-Al_2O_3 substrate (2300 S cm^{-1} [19]) at room temperature. Although ZT of the $Ba_{1/3}CoO_2$ films grown on YSZ substrates was lower (0.058[20]) than that of $Ba_{1/3}CoO_2$ films on (0001) α-Al_2O_3 substrate (0.11[19]) at room temperature, it increased with temperature and reached 0.55 at 600 °C because the grain boundary scattering became less dominant. Therefore, we expect the freestanding $Ba_{1/3}CoO_2$ single-crystalline film to exhibit high ZT values at higher temperatures.

Finally, we discuss κ. In the previous report, we measured κ of the $Ba_{1/3}CoO_2$ epitaxial films using the time-domain thermoreflectance (TDTR) method[29]. Because $Ba_{1/3}CoO_2$ epitaxial films exhibit good electron transport properties in the in-plane direction, κ must be measured in the in-plane direction to extract ZT. Previously, we used the TDTR method to measure the

out-of-plane κ of the $Ba_{1/3}CoO_2$ epitaxial films with two different crystallographic orientations: a *c*-axis orientation and a 55°-inclined *c*-axis.[19, 20] Using these two out-of-plane κ data, we extracted the in-plane κ theoretically.[30] It is very important that the κ value of the freestanding $Ba_{1/3}CoO_2$ single crystalline film measured using the AC calorimetric method agree well with the κ value of the $Ba_{1/3}CoO_2$ epitaxial film measured using the TDTR method.

In summary, we successfully fabricated freestanding $Ba_{1/3}CoO_2$ single-crystalline films by peeling off $Ba_{1/3}CoO_2$ epitaxial films from the substrate. We immersed $Ba_{1/3}CoO_2$ epitaxial films in 40 °C hot water for several tens of minutes to peel off the films. The crystal structures and thermoelectric properties of the peeled films were maintained. The present results provide a useful method for fabricating freestanding single-crystalline oxide films for thermoelectrics.

EXPERIMENTAL

Fabrication of $Ba_{1/3}CoO_2$ epitaxial films. Epitaxial $Ba_{1/3}CoO_2$ films were grown on (0001) α-Al_2O_3 single crystal plates as following. First, CoO epitaxial films (thickness:300 nm, the target thickness of $Ba_{1/3}CoO_2$:600 nm) were grown on (0001) α-Al_2O_3 substrates at 700 °C by a pulsed laser deposition technique (KrF excimer laser, ~2 J cm^{-2} $pulse^{-1}$, 10 Hz). The oxygen pressure was kept at 10^{-3} Pa during the deposition. The CoO film was then heated in $NaHCO_3$ powder at 750 °C in air. After that, we obtained a $Na_{3/4}CoO_2$ epitaxial film. The Na^+ ions in the resulting films were then exchanged with Ba^{2+} ions by heating the $Na_{3/4}CoO_2$ epitaxial films with molten $Ba(NO_3)_2$ and KNO_3 at 500 °C for 1 h. Details of the fabrication procedure have been published elsewhere.[19, 25]

Crystal structure characterization of the films: The thickness, crystallographic orientation, and lattice parameters of the resultant films were analyzed using X-ray diffraction (XRD, Cu $K\alpha_1$ radiation, ATX-G, Rigaku Co.). Out-of-plane diffraction patterns, rocking curves, and X-ray reflection patterns were obtained. The lattice structure of the resulting films was visualized using a high-angle annular dark-field scanning transmission electron microscope (HAADF-STEM; ARM-200F, JEOL).

Measurements of the thermoelectric properties: The σ of the resultant films was measured using the DC four-probe method. The S values of the resultant films were measured using the conventional steady-state method. The uncertainties in thermopower and electrical conductivity were less than 5%, whereas those in thermal conductivity were ~15%. Therefore, the uncertainty in ZT was approximately 20%.

ASSOCIATED CONTENT

Supporting Information is available free of charge via the Internet at https://pubs.acs.org/doi/10.1021/acsaem.XXXXXXX.

In-plane thermal diffusivity measurement; time-dependent temperature at four points for AC thermal frequencies; amplitude of temperature oscillation

AUTHOR INFORMATION

Corresponding Authors

Ichiro Terasaki − Department of Physics, Nagoya University, Furo, Chikusa, Nagoya 464-8602, Japan

ORCiD: orcid.org/0000-0002-6073-2639

Email: terra@nagoya-u.jp

Hyoungjeen Jeen − Department of Physics, Pusan National University, Geumjeong-gu, Busan 46241, Korea

ORCiD: orcid.org/0000-0003-2922-377X

Email: hjeen@pusan.ac.kr

Hiromichi Ohta − Research Institute for Electronic Science, Hokkaido University, N20W10,

Kita, Sapporo 001-0020, Japan

ORCiD: orcid.org/0000-0001-7013-0343

Email: hiromichi.ohta@es.hokudai.ac.jp

Authors

Kungwan Kang − Graduate School of Information Science and Technology, Hokkaido University, N14W9, Kita, Sapporo 060-0814, Japan

ORCiD: orcid.org/0000-0001-5547-8034

Fumiaki Kato − Department of Physics, Nagoya University, Furo, Chikusa, Nagoya 464-8602, Japan

Akitoshi Nakano − Department of Physics, Nagoya University, Furo, Chikusa, Nagoya 464-8602, Japan

ORCiD: orcid.org/0000-0001-9780-5179

Takashi Endo − Research Institute for Electronic Science, Hokkaido University, N20W10, Kita, Sapporo 001-0020, Japan

ORCiD: orcid.org/0000-0003-0642-8748

Yasutaka Matsuo − Research Institute for Electronic Science, Hokkaido University, N20W10, Kita, Sapporo 001-0020, Japan

ORCiD: orcid.org/0000-0002-5071-0284

Author Contributions

K. K. fabricated the samples and measured the thermoelectric properties. K.K., F.K., A.N., and I.T. measured the in-plane thermal diffusivity. T.E. and Y.M. performed STEM observations. H.J. and H.O. planned and supervised the study. All the authors discussed the results and commented on the manuscript.

Funding Sources

K.K. was supported by the JST SPRING (JPMJSP2119). Hiromichi Ohta received funding from the JSPS Grants-in-Aid (19H05788 and 22H00253).

Notes

The authors declare no competing interest.

ACKNOWLEDGMENTS

The authors thank Yuko Mori and Naomi Hirai for the STEM observations. The authors also acknowledge Nozomi Takeda for ICP-MS measurements. This study was supported by Grant-in-Aid for Innovative Areas (19H05791) from the Japan Society for the Promotion of Science (JSPS). K.K. was supported by the JST SPRING (JPMJSP2119). H.O. was supported by a Grant-in-Aid for Scientific Research A (22H00253) from the JSPS. This work was partly supported by the Korea–Japan Bilateral Joint Seminars with NRF and JSPS, the Crossover Alliance to Create the Future with People, Intelligence and Materials, the Network Joint Research Center for Materials and Devices, and the Advanced Research Infrastructure for Materials and Nanotechnology Japan by the Ministry of Education, Culture, Sports, Science and Technology (MEXT).

REFERENCES

(1) Snyder, G. J.; Toberer, E. S. Complex thermoelectric materials. *Nature Mater.* **2008,** 7, 105-114.
(2) He, J.; Tritt, T. M. Advances in thermoelectric materials research: Looking back and

moving forward. *Science* **2017,** 357, eaak9997.
(3) Mahan, G.; Sales, B.; Sharp, J. Thermoelectric Materials: New Approaches to an Old Problem. *Phys. Today* **1997,** 50, 42-47.
(4) Poudel, B.; Hao, Q.; Ma, Y.; Lan, Y. C.; Minnich, A.; Yu, B.; Yan, X. A.; Wang, D. Z.; Muto, A.; Vashaee, D.; Chen, X. Y.; Liu, J. M.; Dresselhaus, M. S.; Chen, G.; Ren, Z. F. High-thermoelectric performance of nanostructured bismuth antimony telluride bulk alloys. *Science* **2008,** 320, 634-638.
(5) Kim, S. I.; Lee, K. H.; Mun, H. A.; Kim, H. S.; Hwang, S. W.; Roh, J. W.; Yang, D. J.; Shin, W. H.; Li, X. S.; Lee, Y. H.; Snyder, G. J.; Kim, S. W. Dense dislocation arrays embedded in grain boundaries for high-performance bulk thermoelectrics. *Science* **2015,** 348, 109-114.
(6) Mamur, H.; Bhuiyan, M.; Korkmaz, F.; Nil, M. A review on bismuth telluride (Bi_2Te_3) nanostructure for thermoelectric applications. *Renew. Sustain. Energy Rev.* **2018,** 82, 4159-4169.
(7) Hsu, K. F.; Loo, S.; Guo, F.; Chen, W.; Dyck, J. S.; Uher, C.; Hogan, T.; Polychroniadis, E. K.; Kanatzidis, M. G. Cubic $AgPb_mSbTe_{2+m}$: Bulk thermoelectric materials with high figure of merit. *Science* **2004,** 303, 818-821.
(8) Heremans, J. P.; Jovovic, V.; Toberer, E. S.; Saramat, A.; Kurosaki, K.; Charoenphakdee, A.; Yamanaka, S.; Snyder, G. J. Enhancement of thermoelectric efficiency in PbTe by distortion of the electronic density of states. *Science* **2008,** 321, 554-557.
(9) Zhao, L.; Tan, G.; Hao, S.; He, J.; Pei, Y.; Chi, H.; Wang, H.; Gong, S.; Xu, H.; Dravid, V. P.; Uher, C.; Snyder, G. J.; Wolverton, C.; Kanatzidis, M. G. Ultrahigh power factor and thermoelectric performance in hole-doped single-crystal SnSe. *Science* **2016,** 351, 141-144.
(10) Chang, C.; Wu, M. K.; He, D.; Pei, Y.; Wu, C. H.; Wu, X. W.; Yu, H.; Zhu, F.; Wang, K.; Chen, Y.; Huang, L.; Li, J.; He, J.; Zhao, L. 3D charge and 2D phonon transports leading to high out-of-plane *ZT* in n-type SnSe crystals. *Science* **2018,** 360, 778-783.
(11) Zhou, C.; Lee, Y.; Yu, Y.; Byun, S.; Luo, Z. L.; Lee, H.; Ge, B.; Lee, Y.; Chen, X.; Lee, J.; Cojocaru-Mirédin, O.; Chang, H.; Im, J.; Cho, S.; Wuttig, M.; Dravid, V. P.; Kanatzidis, M. G.; Chung, I. Polycrystalline SnSe with a thermoelectric figure of merit greater than the single crystal. *Nature Mater.* **2021,** 20, 1378-1384.
(12) Terasaki, I.; Sasago, Y.; Uchinokura, K. Large thermoelectric power in $NaCo_2O_4$ single crystals. *Phys. Rev. B* **1997,** 56, 12685-12687.
(13) Okuda, T.; Nakanishi, K.; Miyasaka, S.; Tokura, Y. Large thermoelectric response of

metallic perovskites: $Sr_{1-x}La_xTiO_3$ ($0 \leq x \leq 0.1$). *Phys. Rev. B* **2001,** 63, 113104.
(14) Ohta, H.; Sugiura, K.; Koumoto, K. Recent progress in oxide thermoelectric materials: p-type $Ca_3Co_4O_9$ and n-type $SrTiO_3$. *Inorg. Chem.* **2008,** 47, 8429-8436.
(15) Fergus, J. W. Oxide materials for high temperature thermoelectric energy conversion. *J. Eur. Ceram. Soc.* **2012,** 32, 525-540.
(16) Koumoto, K.; Funahashi, R.; Guilmeau, E.; Miyazaki, Y.; Weidenkaff, A.; Wang, Y. F.; Wan, C. L. Thermoelectric Ceramics for Energy Harvesting. *J. Am. Ceram. Soc.* **2013,** 96, 1-23.
(17) Liu, J.; Huang, X.; Yang, D.; Xu, G.; Chen, L. Synthesis and physical properties of layered Ba_xCoO_2. *Dalton Trans.* **2014,** 43, 15414.
(18) Liu, J.; Huang, X.; Yang, D.; Wan, S.; Xu, G. High-temperature thermoelectric properties of layered Ba_xCoO_2. *Scripta Mater.* **2015,** 100, 63-65.
(19) Takashima, Y.; Zhang, Y.; Wei, J.; Feng, B.; Ikuhara, Y.; Cho, H. J.; Ohta, H. Layered Cobalt Oxide Epitaxial Films Exhibiting Thermoelectric $ZT = 0.11$ at Room Temperature. *J. Mater. Chem. A* **2021,** 9, 274-280.
(20) Zhang, X.; Zhang, Y.; Wu, L.; Tsuruta, A.; Mikami, M.; Cho, H. J.; Ohta, H. $Ba_{1/3}CoO_2$: A Thermoelectric Oxide Showing a Reliable *ZT* of approximately 0.55 at 600 °C in Air. *ACS Appl. Mater. Interfaces* **2022,** 14, 33355-33360.
(21) Lu, D.; Baek, D. J.; Hong, S. S.; Kourkoutis, L. F.; Hikita, Y.; Hwang, H. Y. Synthesis of freestanding single-crystal perovskite films and heterostructures by etching of sacrificial water-soluble layers. *Nature Mater.* **2016,** 15, 1255-1260.
(22) Kum, H. S.; Lee, H.; Kim, S.; Lindemann, S.; Kong, W.; Qiao, K.; Chen, P.; Irwin, J.; Lee, J. H.; Xie, S.; Subramanian, S.; Shim, J.; Bae, S.; Choi, C.; Ranno, L.; Seo, S.; Lee, S.; Bauer, J.; Li, H.; Lee, K.; Robinson, J. A.; Ross, C. A.; Schlom, D. G.; Rzchowski, M. S.; Eom, C.-B.; Kim, J. Heterogeneous integration of single-crystalline complex-oxide membranes. *Nature* **2020,** 578, 75-81.
(23) Gong, L.; Wei, M.; Yu, R.; Ohta, H.; Katayama, T. Significant Suppression of Cracks in Freestanding Perovskite Oxide Flexible Sheets Using a Capping Oxide Layer. *ACS Nano* **2022,** 16, 21013-21019.
(24) Ohta, H.; Mizutani, A.; Sugiura, K.; Hirano, M.; Hosono, H.; Koumoto, K. Surface modification of glass substrates for oxide heteroepitaxy: Pasteable three-dimensionally oriented layered oxide thin films. *Adv. Mater.* **2006,** 18, 1649.
(25) Ohta, H.; Kim, S. W.; Ohta, S.; Koumoto, K.; Hirano, M.; Hosono, H. Reactive solid-

phase epitaxial growth of Na_xCoO_2 (x ~0.83) via lateral diffusion of Na into a cobalt oxide epitaxial layer. *Cryst. Growth Des.* **2005,** 5, 25-28.
(26) Ohta, S.; Ohta, H.; Koumoto, K. Grain size dependence of thermoelectric performance of Nb-doped $SrTiO_3$ polycrystals. *J. Cerami. Soc. Jpn.* **2006,** 114, 102-105.
(27) Hatta, I.; Sasuga, Y.; Kato, R.; Maesono, A. Thermal diffusivity measurement of thin films by means of an ac calorimetric method. *Rev. Sci. Instrum.* **1985,** 56, 1643-1647.
(28) Kawasaki, S.; Nakano, A.; Taniguchi, H.; Cho, H. J.; Ohta, H.; Nakamura, F.; Terasaki, I. Thermal Diffusivity of the Mott Insulator Ca_2RuO_4 in a Non-equilibrium Steady State. *J Phys Soc Jpn* **2021,** 90, 063601.
(29) Cahill, D. G. Analysis of heat flow in layered structures for time-domain thermoreflectance. *Rev. Sci. Instrum.* **2004,** 75, 5119-5122.
(30) Cho, H. J.; Kim, G.; Onozato, T.; Jeen, H.; Ohta, H. Thermal conductivity tensor of NbO_2. *Int. J. Heat Mass Transf.* **2019,** 137, 263-267.

Table 1. Thermoelectric properties of the freestanding $Ba_{1/3}CoO_2$ single crystalline films at room temperature. The data of the previous reports[19, 20] are also show for comparison.

	This work	Takashima *et al.*[19]	Zhang *et al.*[20]
σ (S cm^{-1})	1,000	2,300	1,100
S (μV K^{-1})	73	72	75
κ (W m^{-1} K^{-1})	3.4	3.3	3.2
ZT	0.047	0.11	0.058

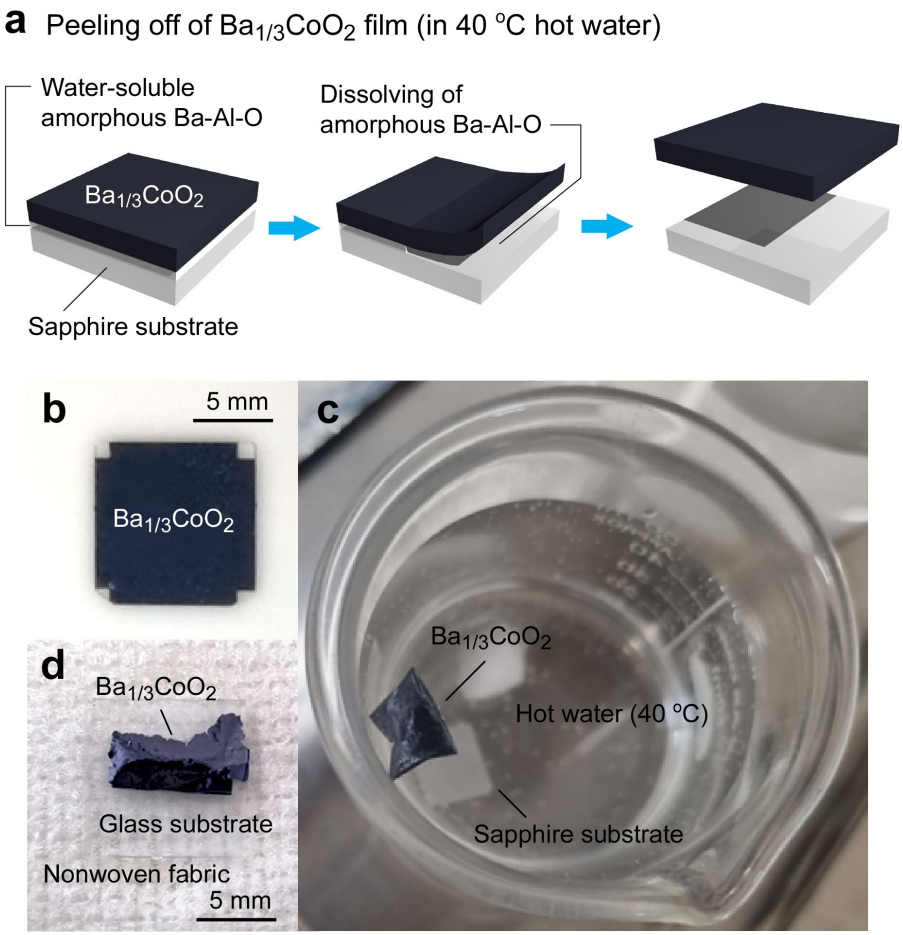

Figure 1. Fabrication of freestanding $Ba_{1/3}CoO_2$ single crystalline films. (a) Peeling-off procedure of $Ba_{1/3}CoO_2$ epitaxial films. We immersed the film in 40 °C hot water. Several tens of minutes later, the amorphous Ba-Al-O layer dissolved in water, and the $Ba_{1/3}CoO_2$ epitaxial film spontaneously peeled off. (b) Photograph of the as-grown $Ba_{1/3}CoO_2$ epitaxial film (~600-nm thick) on the (0001) α-Al_2O_3 substrate. (c) Photograph of the separation of the $Ba_{1/3}CoO_2$ epitaxial film in hot water (40 °C) gives a freestanding $Ba_{1/3}CoO_2$ film. The $Ba_{1/3}CoO_2$ epitaxial film floated on the surface of the water similar to seaweed. (d) Photograph of the peeled-off $Ba_{1/3}CoO_2$ epitaxial film pasted on a glass substrate.

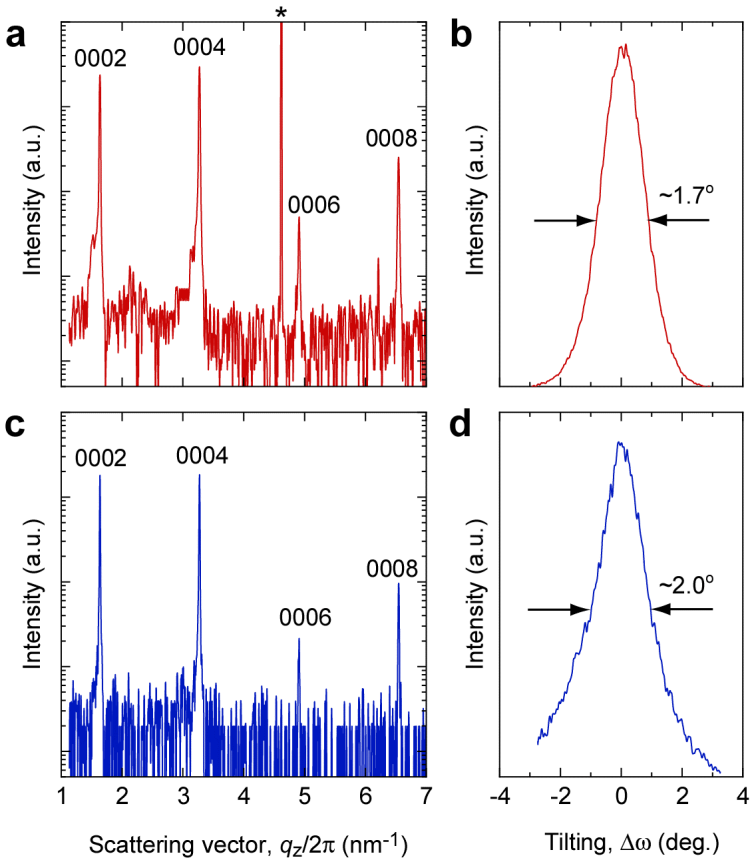

Figure 2. Comparison of the XRD patterns of the $Ba_{1/3}CoO_2$ films before and after peeled-off. Out-of-plane XRD patterns of (a) the as-grown $Ba_{1/3}CoO_2$ epitaxial film and (c) the peeled-off film on the glass substrate. Intense diffraction peaks of 000*l* $Ba_{1/3}CoO_2$ are seen before and after being peeled. Note that there is a substrate peak (*) in (a) but not in (c). Out-of-plane X-ray rocking curves of the 0002 diffraction peak of (b) the as-grown $Ba_{1/3}CoO_2$ epitaxial film and (d) the peeled-off film on a glass substrate. FWHM of the rocking curve slightly increased after being peeled.

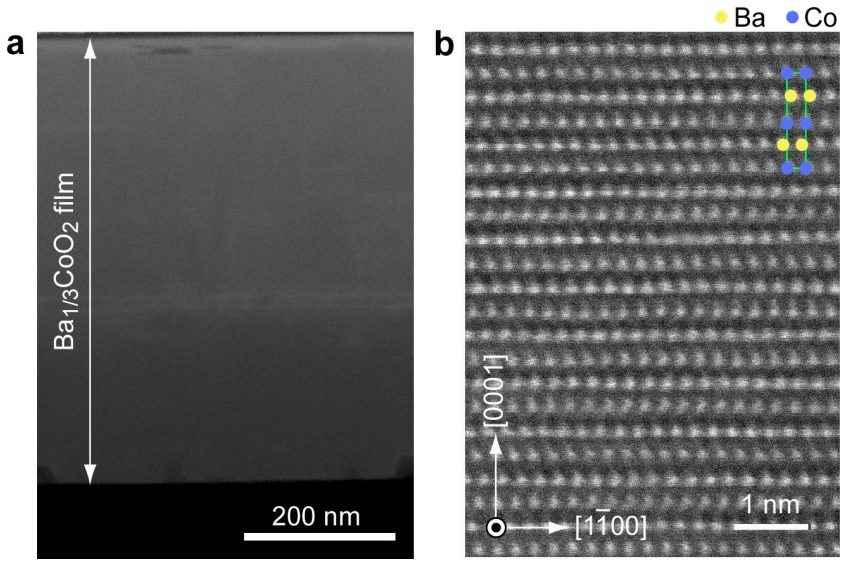

Figure 3. Microstructure of the peeled-off $Ba_{1/3}CoO_2$ epitaxial film. (a) Cross-sectional HAADF-STEM image. Overall thickness is ~600 nm. (b) Magnified HAADF-STEM image. A layered crystal structure composed of alternating CoO_2 (blue-filled circle) and Ba (yellow-filled circle) layers along the *c*-axis is clearly seen.

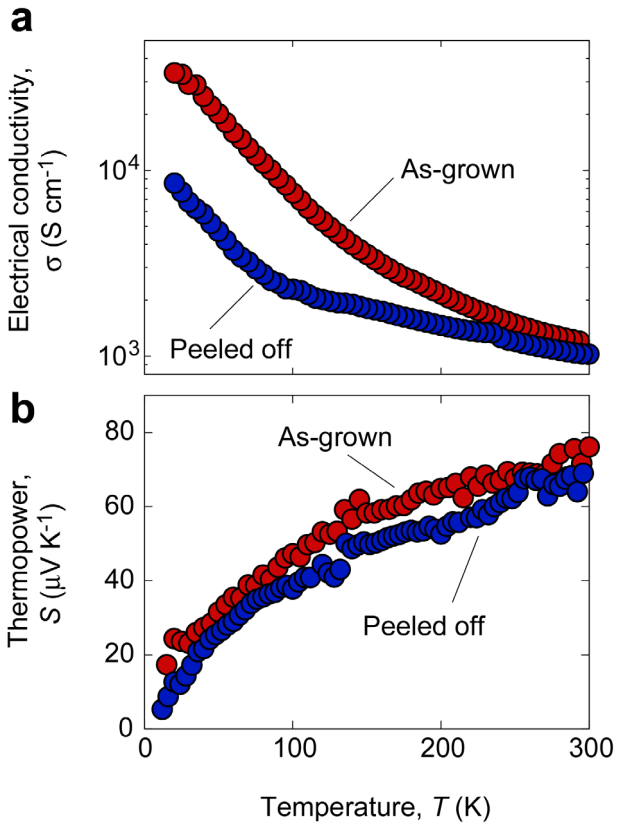

Figure 4. Thermoelectric properties. Temperature dependence of (a) electrical conductivity and (b) thermopower for the $Ba_{1/3}CoO_2$ films before and after peeled-off. The room-temperature σ of the as-grown $Ba_{1/3}CoO_2$ film was ~1100 S cm^{-1}, while that of after peeled-off was ~1000 S cm^{-1}. Both films exhibited metallic conductivity. The room-temperature *S* of the as-grown film was +76 μV K^{-1}, while that of the one after being peeled was +73 μV K^{-1}. The S values of both films gradually decreased as the temperature decreased, demonstrating that the peeling-off treatment does not affect the thermoelectric properties.

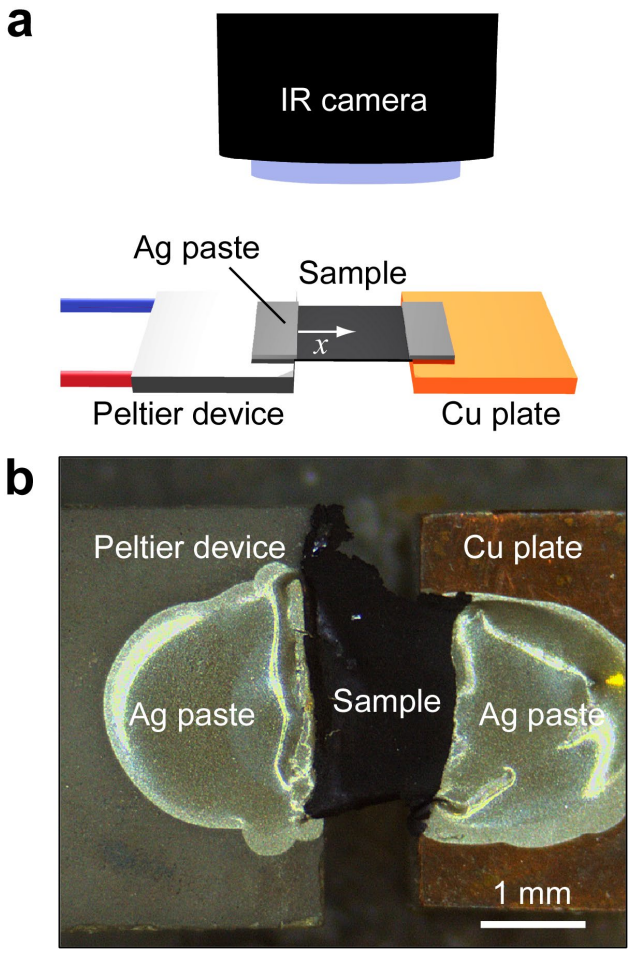

Figure 5. Measurement setup for the In-plane thermal diffusivity of the freestanding $Ba_{1/3}CoO_2$ single crystalline films. (a) Schematic illustration. (b) Photograph of the equipment.

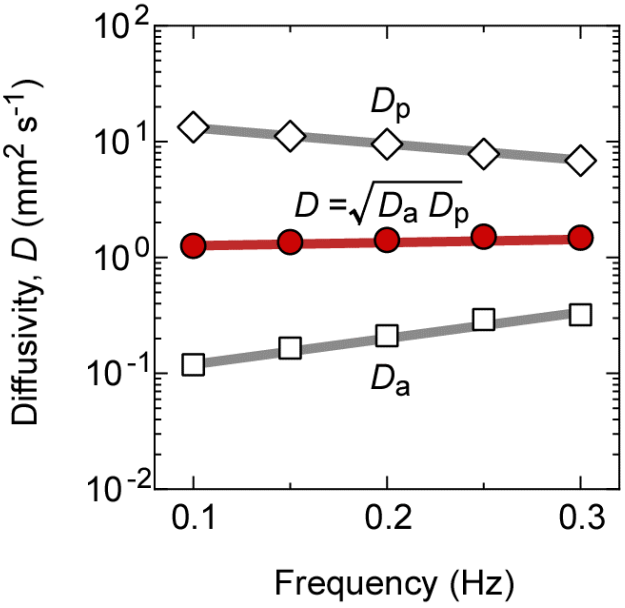

Figure 6. In-plane thermal diffusivity (D) of the freestanding $Ba_{1/3}CoO_2$ single crystalline films. The D values were obtained as $(D_a \cdot D_p)^{1/2}$. D of the freestanding $Ba_{1/3}CoO_2$ single crystalline films was 1.45 mm^2 s^{-1} at room temperature. Consequently, κ (= $C_p \cdot \rho \cdot D$) of the freestanding $Ba_{1/3}CoO_2$ single crystalline films was ~3.4 W m^{-1} K^{-1}, which is consistent with that of the as-grown film (~3.2 W m^{-1} K^{-1}).

For Table of Contents Use Only

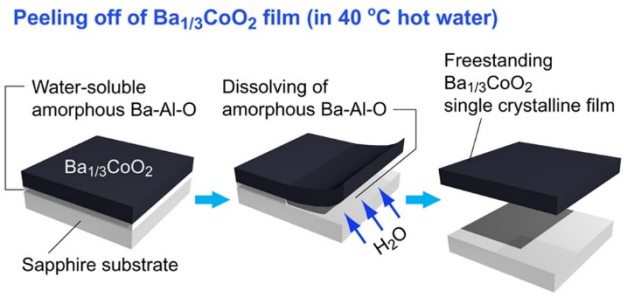

Supporting Information

Fabrication and Thermoelectric Properties of Freestanding $Ba_{1/3}CoO_2$ Single Crystalline Films

Kungwan Kang[1], Fumiaki Kato[2], Akitoshi Nakano[2], Ichiro Terasaki[2,*], Takashi Endo[3], Yasutaka Matsuo[3], Hyoungjeen Jeen[4,*], and Hiromichi Ohta[3,*]

[1] *Graduate School of Information Science and Technology, Hokkaido University, N14W9, Kita, Sapporo 060-0814, Japan*

[2] *Department of Physics, Nagoya University, Furo, Chikusa, Nagoya 464-8602, Japan*

[3] *Research Institute for Electronic Science, Hokkaido University, N20W10, Kita, Sapporo 001-0020, Japan*

[4] *Department of Physics, Pusan National University, Geumjeong-gu, Busan 46241, Korea*

*Emails: terra@nagoya-u.jp, hjeen@pusan.ac.kr, hiromichi.ohta@es.hokudai.ac.jp

S1. In-plane thermal diffusivity measurement

We employed a sine wave heating and cooling method using a Peltier device to measure the in-plane thermal diffusivity of a sample. A Peltier device is placed to one side of the sample. The Peltier device generates a thermal wave that propagates through the material. Consequently, a corresponding local temperature wave, $T(x, t)$, is observed at position x from the edge of the device at time t. The $T(x, t)$ is determined based on the conventional heat conduction theory.

$$c\frac{\partial T}{\partial t} + \frac{2\delta}{d}(T - T_0) - \kappa\frac{\partial^2 T}{\partial x^2} = \frac{Q_0 e^{i\omega t}}{d} \tag{S1}$$

Where c is the specific heat per sample volume. The second term from the left represents the thermal conduction to the heat bath. where δ is the thermal conductance per unit area between the Peltier device and the bottom of the sample, d is the sample thickness, and T_0 is the temperature of the Peltier element surface. The right side represents the external heat flux, where $Q_0 e^{i\omega t}$ is the AC heat flux per unit area from the Peltier device to the sample.

A wave-form solution for Eq. S1 is given by,

$$T(x,t) = \Delta T(x)\sin\big(2\pi f t - \phi(x)\big) + T_0 \tag{S2}$$

The amplitude (ΔT) and phase (ϕ) are given by,

$$\Delta T = \frac{Q_0}{2\omega c d\sqrt{1 + (\omega\tau)^2}} e^{-k_a x} \tag{S3}$$

$$\phi = k_p x + \phi_0 \tag{S4}$$

k_a and k_p can be calculated from the amplitude and phase of the observed temperature oscillation as

$$k_a = -\frac{d(ln\Delta T(x))}{dx} = -\frac{ln\Delta T(x_2) - ln\Delta T(x_1)}{x_2 - x_1} \tag{S5}$$

$$k_p = \frac{d(\phi(x))}{dx} = \frac{\phi(x_2) - \phi(x_1)}{x_2 - x_1} \tag{S6}$$

Using the experimental data, k_a and k_p are obtained, and the frequency dependent

thermal diffusivities D_a and D_p are given by,

$$D_i = \frac{\omega}{2k_i^2} \ (i = a \text{ and } b) \tag{S7}$$

Finally, the thermal diffusivity (D) is obtained as

$$D = \sqrt{D_a D_p} \tag{S8}$$

Figures S1a and **S1b** illustrate $T(x, t)$ for a range of x values from 0.1 mm to 0.5 mm, corresponding to frequencies of 0.10 Hz and 0.30 Hz.

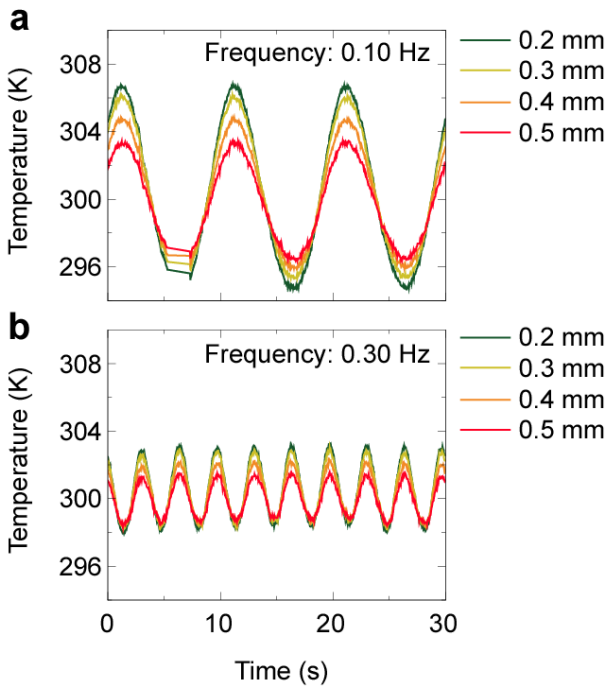

Figure S1. Time-dependent temperature at four points for ac thermal frequencies of (a) 0.10 Hz and (b) 0.30 Hz.

To determine the amplitude (ΔT) and phase difference ($\Delta\phi$) at various positions and frequencies, we employ Eq. S2 and perform fitting procedures. The resulting values of ΔT and $\Delta\phi$ are then presented as functions of x in **Figs S2a** and **S2b**, respectively.

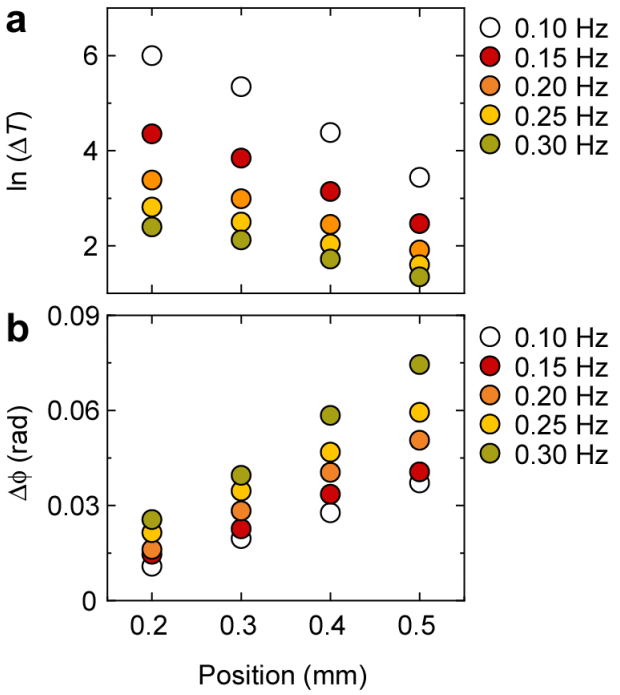

Figure S2. The amplitude of the temperature oscillation is represented in (a), and the phase is shown in (b) as a function of position *x*.

The values of D_a and D_p obtained from k_a and k_p are represented as functions of frequency in **Fig. 6**, and the thermal diffusivity D is determined to be 1.45 mm^2 s^{-1}. The thermal conductivity (κ) was determined using a straightforward equation ($\kappa = D \cdot \rho \cdot C_p$), where ρ denotes the density, κ stands for thermal conductivity, and C_p represents the specific heat capacity. By using a bulk density (ρ) value of 5.36 g cm^{-3} and a specific heat capacity (C_p) value of 0.44 J g^{-1} K^{-1}, we calculated the in-plane thermal conductivity (κ) to be 3.45 W m^{-1} K^{-1}.